



Tuning the selectivity of photothermal CO₂ hydrogenation through photo-induced interaction between Ni nanoparticles and TiO₂

Jun Ma ^{a,b,1}, Tianyang Liu ^{c,1}, Guangyu Chen ^a, Shengkun Liu ^a, Wanbing Gong ^a, Yu Bai ^a, Hengjie Liu ^a, Yu Wang ^{c,*}, Dong Liu ^{a,b,**}, Ran Long ^a, Yafei Li ^c, Yujie Xiong ^{a,b,***}

^a Key Laboratory of Precision and Intelligent Chemistry, School of Chemistry and Materials Science, Hefei National Research Center for Physical Sciences at the Microscale, National Synchrotron Radiation Laboratory, School of Nuclear Science and Technology, University of Science and Technology of China, Hefei, Anhui 230026, PR China

^b Suzhou Institute for Advanced Research, University of Science and Technology of China, Suzhou, Jiangsu 215123, PR China

^c Jiangsu Collaborative Innovation Centre of Biomedical Functional Materials, School of Chemistry and Materials Science, Nanjing Normal University, Nanjing, Jiangsu 210023, PR China



ARTICLE INFO

Keywords:

Photothermal catalysis
Selective hydrogenation
Strong metal-support interactions
CO₂ conversion
Electronic structure

ABSTRACT

Photothermal CO₂ hydrogenation into value-added chemicals driven by abundant solar energy is a promising and sustainable approach for achieving carbon neutralization. Herein, we demonstrate the photo-induced interaction between Ni nanoparticles and TiO₂ support (Ni@TiO₂) for maneuvering the selectivity of photothermal CO₂ hydrogenation. According to experimental characterizations and theoretical simulations, the formed strong metal-support interaction between Ni and TiO₂ can significantly enhance the adsorption of key intermediate *CO for further hydrogenation, thus tuning the CO₂ hydrogenation pathway toward CH₄. Consequently, the Ni@TiO₂ catalyst exhibits a CH₄ production rate of 286.5 mmol g_{cat}⁻¹ h⁻¹ with an 81.8% selectivity under full-spectrum solar light irradiation. Moreover, in situ experimental characterizations and theoretical calculations suggest that photothermal CO₂ hydrogenation over Ni@TiO₂ undergoes a stepwise hydrogenation pathway to methane. This work offers insights into a simple approach for designing efficient nonprecious metal-based CO₂ methanation catalysts.

1. Introduction

To ameliorate the issues of fossil fuel dependence and global warming, there is an urgent need to advance the development of sustainable technologies for clean energy supply and CO₂ fixation.^[1–4] Recently, there has been a surge of interest and attention from the scientific community toward solar-driven CO₂ conversion. This process can effectively mitigate energy crisis and climate emergency synchronously by utilizing abundant and widely available solar energy to produce chemicals and fuels.^[5,6] In particular, photothermal catalytic CO₂ hydrogenation can transduce photons into heat to locally raise the surface temperature of the catalysts and further efficiently convert CO₂ into value-added chemicals such as CO and CH₄.^[7–10] Among those

products, CH₄ generated from the Sabatier reaction (CO₂ + 4 H₂ ↔ CH₄ + 2 H₂O, ΔG_{298 K}⁰ = -114 kJ mol⁻¹) shows significant practical potentials since it can be directly integrated into the readily available natural gas pipelines and used as raw materials for chemical commodity manufacture.^[2,11,12] Moreover, photothermal CO₂ methanation can be applied as an ideal model reaction to investigate the initial steps of CO₂ hydrogenation.^[13,14] For example, Li and coworkers developed a Ru-supported Ni₂V₂O₇ catalyst for photothermal Sabatier reaction and achieved a CO₂ methanation rate of 114.9 mmol g_{cat}⁻¹ h⁻¹.^[15] Ye and coworkers embedded Ru nanoparticles on exfoliated layered double hydroxides for photothermal CO₂ methanation. Their findings indicated that the catalyst exhibited high-efficiency performance, which was proven to be a result of targeting activation of CO₂ and H₂ over the

* Corresponding author.

** Corresponding authors at: Key Laboratory of Precision and Intelligent Chemistry, School of Chemistry and Materials Science, Hefei National Research Center for Physical Sciences at the Microscale, National Synchrotron Radiation Laboratory, School of Nuclear Science and Technology, University of Science and Technology of China, Hefei, Anhui 230026, PR China.

E-mail addresses: yu.wang@njnu.edu.cn (Y. Wang), dongliu@ustc.edu.cn (D. Liu), yixiong@ustc.edu.cn (Y. Xiong).

¹ These authors contributed equally.

support and Ru nanoparticle components, respectively.^[16] Notwithstanding the notable advancements, the substantial cost and limited availability of noble metals (e.g., Ru, Rh) still hinder the large-scale application of photothermal CO₂ methanation.^[12,17,18]

Recently, there has been significant research interest in the utilization of transition metal (e.g., Co, Ni)-supported catalysts for photothermal CO₂ hydrogenation reaction due to their cost-effectiveness and abundant availability. These catalysts can effectively convert sunlight into heat, and generate a strong surface plasmonic resonance (SPR)-induced electric field for assisting the activation of reactant molecules.^[19–22] For instance, Feng et al. demonstrated that a Co plasmonic hybridization approach could achieve nearly 100% sunlight harvesting and an unprecedented CO production rate of 498.9 mmol g⁻¹ h⁻¹.^[23] However, most of those works focused on breaking one C=O bond of CO₂ to generate CO, i.e., reserve water-gas shift (CO₂ + H₂ ↔ CO + H₂O) reaction. Precisely steering the CO₂ hydrogenation process and controlling the selectivity toward CH₄ remain challenging.^[8,24]

It is well recognized that the binding strength between key intermediates and catalytic sites is decisive for product selectivity.^[25–27] As for CO₂ hydrogenation, strong binding of the intermediates on catalyst surfaces can dramatically promote further hydrogenation of CO₂ molecule and boost CH₄ production via the methanation reaction rather than CO production.^[13,14,28] Generally, surface engineering can be employed to rationally regulate the surface adsorption characteristic of CO₂ hydrogenation reaction. Therefore, the classical strong metal-support interaction (SMSI) holds a significant influence on the catalytic performance and durability through altering the geometry and electrical properties of metal nanoparticles. Consequently, it is plausible that SMSI plays a crucial role in regulating both the activity and selectivity of chemical reactions.^[29–34]

Herein, we developed a photo-induced approach to construct SMSI between Ni nanoparticles (NPs) and TiO₂ (Ni@TiO₂) to maneuver the CH₄ selectivity of photothermal CO₂ hydrogenation. The formed interaction between Ni NPs and TiO₂ can not only enhance the CO₂ reactant adsorption but also increase the adsorption of *CO and *CHO intermediates on the catalysts, which directs the pathway of CO₂ hydrogenation toward CH₄ production. Consequently, the Ni@TiO₂ catalyst exhibits a CH₄ production rate of 286.5 mmol g_{cat}⁻¹ h⁻¹ with 81.8% selectivity under illumination. Additionally, both the activity and selectivity of photothermal CO₂ methanation over Ni@TiO₂ were well sustained over 20 successive cycles. Moreover, the spectral and theoretical investigations revealed that the CO₂ methanation over Ni@TiO₂ undergoes a stepwise hydrogenation pathway. This work presents a novel strategy for enhancing the efficiency of photothermal CO₂ methanation by utilizing full-spectrum solar energy.

2. Experimental section

2.1. Catalyst preparation

The NiO@TiO₂ was synthesized through a sol-gel and subsequent pyrolysis method. Typically, 3.6 g of F127 was dissolved in 36 mL ethanol under continual stirring. Subsequently, 2.72 mL Ti(OBu)₄ (i.e., 8 mmol of Ti) and 0.58 g Ni(NO₃)₂•6 H₂O (i.e., 2 mmol of Ni) were added into the above solution, and the mixture was vigorously stirred for 30 min. Then, 2.3 mL glacial acetic acid and 2 mL hydrochloric acid were added under stirring. After that, the mixture was stirred for 1 h and then transferred into a petri dish (125 mm in diameter). The ethanol was evaporated on a hotplate at 40 °C for 12 h to form a transparent membrane, and it was then aged in a 65 °C oven for 24 h. Finally, the gel was calcined at 450 °C for 5 h with a ramp rate of 2 °C min⁻¹ to obtain NiO@TiO₂ nanostructure catalyst. The NiO@TiO₂ with different Ni/Ti molar ratios were prepared by varying the ratio of Ni(NO₃)₂•6 H₂O and Ti(OBu)₄. The Ni@TiO₂ was prepared via the photoreduction of NiO@TiO₂ in the atmosphere of CO₂ and H₂ mixed gas (20/80 vol%) under light illumination. The light intensity was fixed at 2.5 W cm⁻² and

the illumination time was fixed at 5 min for all the NiO@TiO₂ samples.

2.2. Catalysts characterization

Scanning electron microscopy (SEM) images were taken on a Zeiss Supra 40 field-emission scanning electron microscope at 2.0 kV. Transmission electron microscopy (TEM) images were taken on a Hitachi Model H7700 microscope at 100.0 kV. High-resolution TEM (HRTEM) images, scanning TEM (STEM) images, and energy-dispersive X-ray spectroscopy (EDS) mapping profiles were recorded on an FEI Talos F200X field-emission high-resolution transmission electron microscope at 200.0 kV.

Powder X-ray diffraction (XRD) patterns were recorded by using a Philips X'Pert Pro Super X-ray diffractometer with Cu-K α radiation ($\lambda = 1.54178 \text{ \AA}$).

X-ray photoelectron spectra (XPS) were collected on an ESCALAB 250 X-ray photoelectron spectrometer, using non-monochromatic Al-K α X-ray as the excitation source.

UV-vis-NIR diffuse reflectance spectra were recorded in the spectral region of 200–2500 nm with a Shimadzu SolidSpec-3700 spectrophotometer.

2.3. Gas adsorption analysis

Temperature-programmed desorption of CO was carried out on a Micromeritics AutoChem II 2920 apparatus. The 70 mg of sample was first pretreated at 200 °C in helium for 1 h and then cooled to room temperature. Subsequently, the sample was saturated in a 10 vol% CO/He atmosphere at 50 °C for 1 h and then flushed with helium flow to remove any physisorbed molecules. Finally, the CO desorption was measured in 30 mL min⁻¹ helium flow in the range of 50–700 °C with a heating ramp of 10 °C min⁻¹. Temperature-programmed desorption of CO₂ and CH₄ was performed on the same apparatus with similar procedures. H₂-temperature programmed reduction (H₂-TPR) was carried out on a Micromeritics AutoChem II 2920 apparatus. The 100 mg of sample was first pretreated at 200 °C in helium for 1 h and then cooled to room temperature. Subsequently, the sample was heated from 50 to 700 °C in the flow of 10 vol% H₂/Ar with a heating ramp of 10 °C min⁻¹. The consumption of H₂ was determined by a thermal conductivity detector (TCD).

2.4. Photothermal CO₂ hydrogenation measurements

Photothermal CO₂ hydrogenation was performed in a batch quartz reactor with a total volume of 35 mL. The catalyst was dispersed in an air-permeable quartz fiber filter with an illuminated area of 1.0 cm². The reactor was purged with the CO₂ and H₂ mixed gas (20/80 vol%) for 10 min and then sealed. Then the reactor system was irradiated under a full spectrum xenon lamp (PLS SXE300, Perfect light, China). The light intensity on the sample surface was measured to be 2.5 W cm⁻² by an optical power meter. The temperature of the catalyst surface during photothermal CO₂ conversion was monitored by a K-type thermocouple. After reaction for 10 min, the products were analyzed by gas chromatography (GC, 7890B, Agilent) equipped with a thermal conductor detector (TCD) and flame ionization detector (FID).

3. Results and discussions

3.1. Synthesis and structure characterizations

The Ni@TiO₂ catalyst was prepared by a simple sol-gel method and in situ photoreduction. As illustrated in Fig. S1, NiO@TiO₂ was first synthesized through the sol-gel method using tetrabutyl orthotitanate and Ni(NO₃)₂ as precursors. Subsequently, Ni@TiO₂ can be obtained from in situ photoreduction of NiO@TiO₂ in the atmosphere of CO₂ and H₂ mixed gas (20/80 vol%) under light irradiation. The X-ray diffraction

(XRD) characterization was initially applied to determine the phase changes of the as-prepared samples before and after photoreduction. The XRD patterns of $\text{NiO}@\text{TiO}_2$ (Fig. 1a) exhibit distinct NiO peaks (PDF#47-1049) and characteristic anatase TiO_2 peaks (PDF#72-1148). Upon 5 min of photoreduction, the diffraction patterns associated with NiO phase disappear, and the diffraction patterns corresponding to metallic Ni (PDF#70-0989) become evident. Specifically, the characteristic peaks at 44.6° and 51.9° are attributed to (111) and (200) planes of metallic Ni , respectively. These results confirm that the NiO phase was completely transformed into a metallic Ni phase. Meanwhile, the anatase TiO_2 phase remains unchanged after photoreduction. In addition, the referenced samples with different Ni/Ti molar ratios ($\text{Ni}@\text{TiO}_2-X$, where X is the molar ratio of Ni and Ti in the precursors) show comparable results upon photoreduction (Fig. S2). After confirming the metallic nickel phase of the prepared catalyst, electron microscopy images (Figs. S3,4) reveal the structure of the $\text{Ni}@\text{TiO}_2$ catalyst. Ni nanoparticles with an average size of 20 nm are uniformly loaded on TiO_2 as shown in Fig. S3. Fig. 1b and S4 reveal that a thin TiO_2 overlayer is observed covering Ni NPs, manifesting the formation of SMSI between Ni NPs and TiO_2 support, which is rather different from the Ni -loaded TiO_2 (Ni/TiO_2) sample (Fig. S6). As shown in Fig. 1c, the lattice fringes of 0.179 and 0.208 nm can be assigned to the (200) and (111) planes of Ni , respectively, and the lattice fringe of 0.350 nm is assigned to TiO_2 (100) plane. Moreover, the scanning transmission electron microscopy (STEM) and corresponding elemental mappings for $\text{Ni}@\text{TiO}_2$ based on energy-dispersive X-ray spectroscopy (EDS) (Fig. S7) show the distribution of Ni , Ti , and O elements, as well as the presence of Ni NPs that are partially covered by TiO_2 layer.

Furthermore, the SMSI can be efficiently confirmed by H_2 -temperature programmed reduction (H_2 -TPR) characterization. As displayed in Fig. 1d, a prominent reduction peak around $290\text{--}480^\circ\text{C}$ can be detected for $\text{NiO}@\text{TiO}_2$ or conventional NiO/TiO_2 , corresponding to the

reduction of NiO to Ni phase.^[35,36] Specifically, the temperature of the reduction peak for $\text{NiO}@\text{TiO}_2$ (398°C) is substantially higher than that of NiO/TiO_2 (347°C), indicating stronger interaction between nickel oxide and TiO_2 support in $\text{NiO}@\text{TiO}_2$ samples. Generally, such a strong interaction would significantly improve the subsequent catalytic activity and durability.^[37-39] X-ray photoelectron spectroscopy (XPS) was conducted to analyze the presence of Ni and TiO_2 species. Specifically, the high-resolution Ni 2p XPS spectra (Fig. S8a) exhibit the characteristic peaks at 852.5, 855.8, and 861.1 eV, corresponding to Ni^0 , NiO_x , and satellite peak of NiO_x , respectively, while Ti 2p XPS spectra show typical peaks for TiO_2 (Fig. S8b).

Upon recognizing the structural information of the as-prepared $\text{Ni}@\text{TiO}_2$, the finite-difference time-domain (FDTD) simulations were further conducted to investigate the influence of the strong interaction on the localized electric field distributions for Ni NPs under light irradiation with a wavelength of 350 nm. As shown in Fig. 2a,b, the spatially non-homogeneous electric fields for both Ni NPs and $\text{Ni}@\text{TiO}_2$ show the highest intensity at the surface of the particles and exponentially decrease with the distance from the surface. Interestingly, the intensity of the localized electric field for Ni NPs is dramatically enhanced upon the encapsulation of the TiO_2 layer, which indicates that the interaction between TiO_2 and Ni NPs can significantly boost the plasmonic coupling effect of Ni NPs.^[1,40,41] The enhanced coupling effect can further locally heat the catalyst to high temperature for CO_2 hydrogenation reaction. Afterward, the ultraviolet-visible-near-infrared (UV-vis-NIR) diffuse reflectance spectroscopy was carried out to evaluate the light adsorption ability of the as-prepared samples, which is a substantial parameter for photothermal catalysis. Impressively, the as-prepared $\text{Ni}@\text{TiO}_2$ sample achieves efficient light absorption throughout the full solar spectrum from 200 to 2500 nm (Fig. 2c and S9). In contrast, Ni NPs and Ni/TiO_2 samples show much weaker absorption in the IR regions. The results suggest a significant enhancement in the utilization

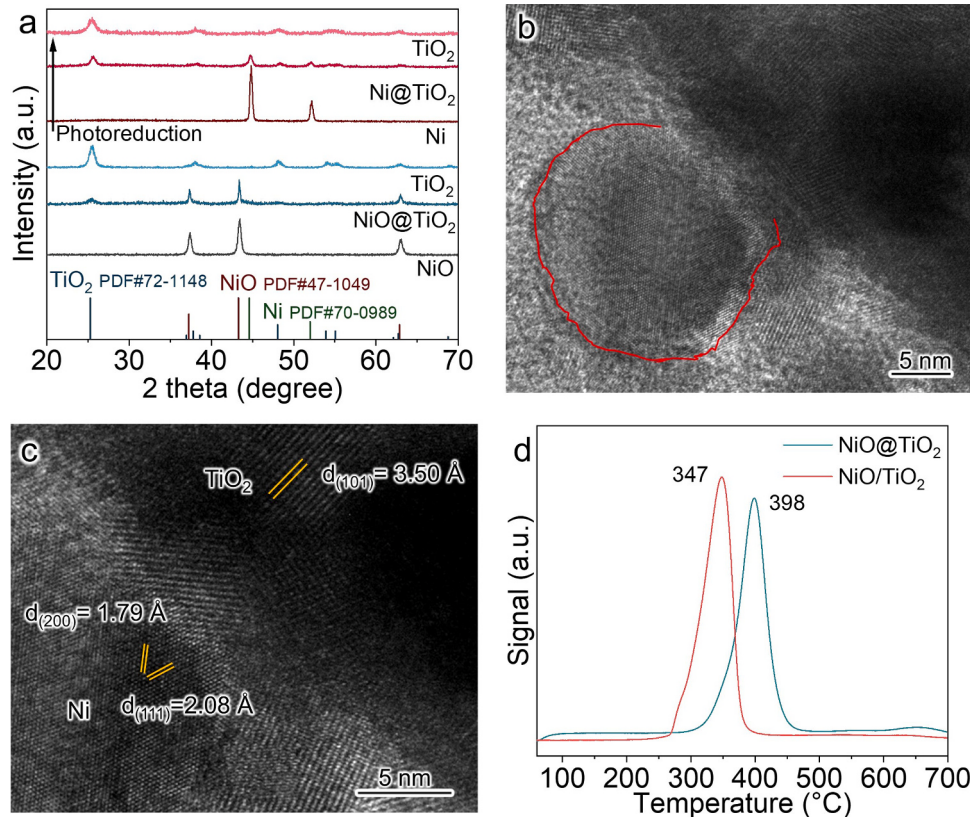


Fig. 1. (a) XRD patterns for the prepared $\text{NiO}@\text{TiO}_2$ and $\text{Ni}@\text{TiO}_2$ catalyst. (b,c) HRTEM images of the as-prepared $\text{Ni}@\text{TiO}_2$ catalyst. (d) H_2 -TPR profiles for $\text{NiO}@\text{TiO}_2$ and NiO/TiO_2 samples.

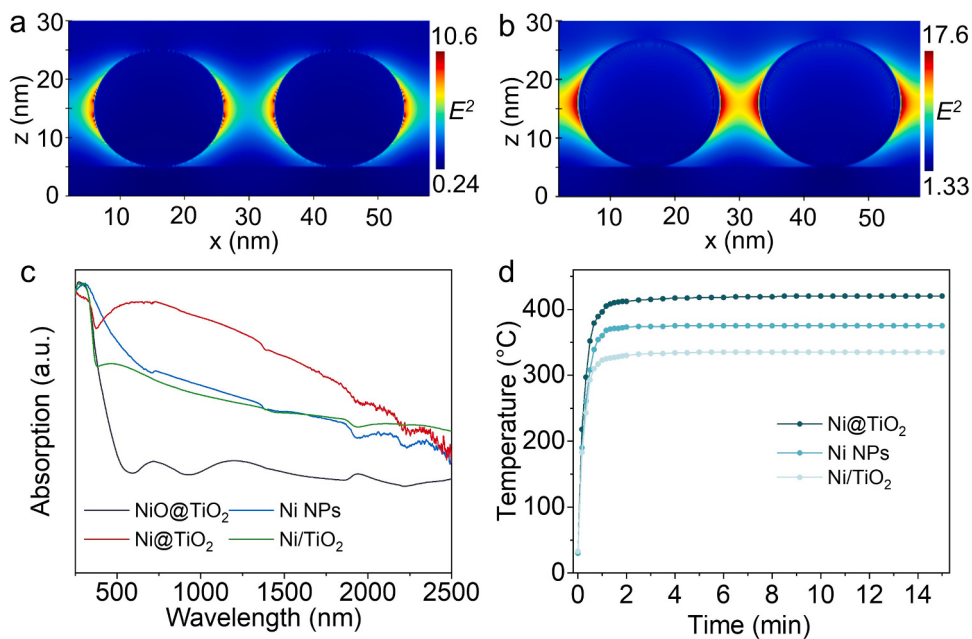


Fig. 2. (a) The distribution of electric field intensity for (a) Ni NPs and (b) Ni NPs encapsulated by TiO₂ layers. (c) UV-vis–NIR absorption spectra of as-synthesized Ni@TiO₂ and reference samples. (d) The photothermal temperature monitoring for Ni@TiO₂, Ni/TiO₂, and bare Ni NPs under 2.5 W cm⁻² illumination in the atmosphere of CO₂ and H₂ mixed gas (20/80 vol%).

efficiency of solar energy upon the formation of the interaction between TiO₂ and Ni NPs. To further explore the photothermal effect, we detected the surface temperatures of the as-obtained samples using an intimate contacting thermocouple under 2.5 W cm⁻² full spectrum light illumination. As displayed in Fig. 2d, the surface temperatures of the samples are increased rapidly within the initial 1 min and peak after about 2 min of illumination. Impressively, Ni@TiO₂ achieves the highest surface photothermal temperature (420 °C), which is appreciably higher than those of Ni/TiO₂ (375 °C) and bare Ni NPs (335 °C),

respectively. In particular, the observed trend in the measured photothermal temperature for these catalysts remains consistent with their light absorption ability, manifesting the enhanced photothermal effect benefiting from the SMSI. Furthermore, the surface temperatures of Ni@TiO₂ can reach 213, 324, 420, and 469 °C under an irradiation intensity of 0.5, 1.5, 2.5, and 3.5 W cm⁻², respectively (Fig. S10). Overall, a simple approach has been effectively employed to synthesize TiO₂–supported Ni NPs catalyst exhibiting SMSI with highly improved photothermal effect, rendering potential for some promising photothermal

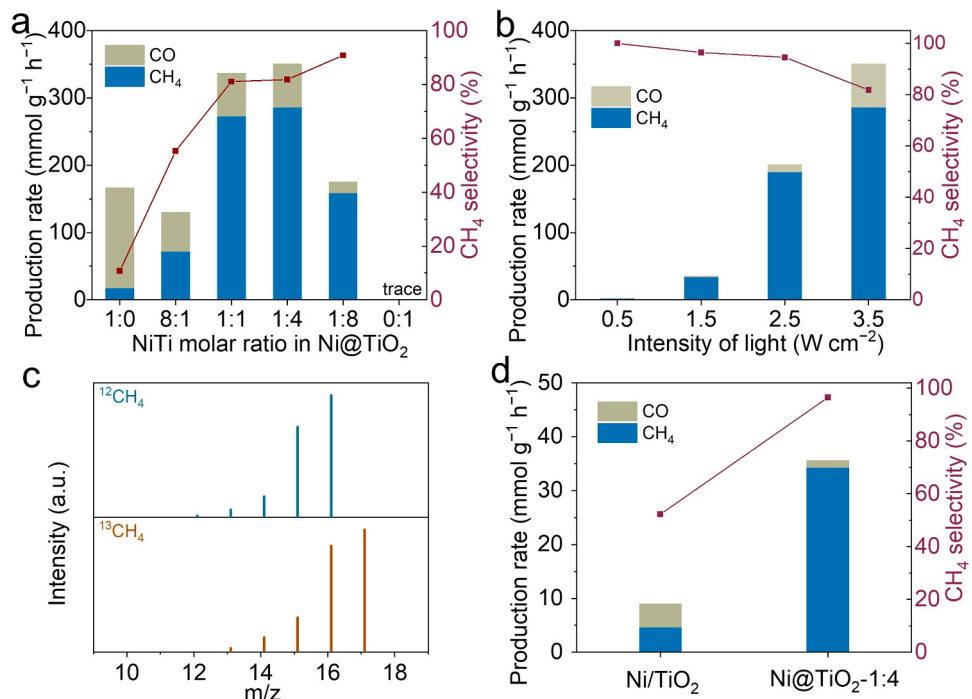


Fig. 3. (a) The photothermal CO₂ hydrogenation performance over Ni@TiO₂ catalysts under a 3.5 W cm⁻² illumination. (b) The photothermal CO₂ hydrogenation performance over Ni@TiO₂ catalyst under different irradiation intensities. (c) GC–MS spectra of the produced CH₄ over Ni@TiO₂ using ¹²CO₂ and ¹³CO₂ as reactants. (d) The production rate and CH₄ selectivity for photothermal CO₂ hydrogenation over Ni@TiO₂ and Ni/TiO₂ under a 1.5 W cm⁻² illumination.

catalytic applications.

3.2. Photothermal CO₂ hydrogenation performance

After acknowledging the remarkable plasmonic-induced photothermal effect of Ni@TiO₂ catalyst, we further evaluated its catalytic performance for photothermal CO₂ hydrogenation. Photothermal CO₂ hydrogenation reactions were performed in a homemade quartz batch reactor feeding with H₂ and CO₂ at a molar ratio of 4:1 under full-spectrum illumination. As shown in Fig. 3a, Ni@TiO₂ catalysts achieve efficient performance on photothermal CO₂ hydrogenation, producing CO and CH₄. Specifically, bare Ni NPs catalyst achieves a CO production rate of 166.0 mmol g_{cat}⁻¹ h⁻¹ with 89.2% CO selectivity under 3.5 W cm⁻² illumination. Moreover, the CO₂ conversion over Ni@TiO₂ is over 93% after 10 min of reaction under a 3.5 W cm⁻² illumination. In sharp contrast, Ni@TiO₂-1:4 catalyst produces a high CH₄ production rate of 286.5 mmol g_{cat}⁻¹ h⁻¹ with 81.8% CH₄ selectivity under 3.5 W cm⁻² illumination, while the bare TiO₂ catalyst yields virtually undetectable levels of products. It is worth noting that increasing the TiO₂ amount in Ni@TiO₂ catalyst can tune the selectivity of photothermal CO₂ hydrogenation toward CH₄. In other words, these results indicate that establishing and reinforcing the SMSI interaction between Ni NPs with TiO₂ support are essential factors in facilitating photothermal CO₂ hydrogenation and directing the reaction toward the production of CH₄.

Thereafter, the photothermal CO₂ hydrogenation performance over Ni@TiO₂-1:4 was studied under different irradiation intensities. Specifically, negligible CH₄ and CO could be observed under 0.5 W cm⁻² illumination (Fig. 3b) due to the relatively lower photothermal temperature. The CH₄ production rate is greatly promoted from 34.3 to 189.9 mmol g_{cat}⁻¹ h⁻¹ as the illumination intensity increases from 1.5 to 2.5 W cm⁻², and then CH₄ production rate reaches 286.5 mmol g_{cat}⁻¹ h⁻¹ under an irradiation intensity of 3.5 W cm⁻². It is worth noting that the selectivity toward CH₄ gradually decreases as the intensity of the irradiated light increases, whereas the CH₄ selectivity gradually declines from 94.6% to 81.8% as the illumination intensity increases from 1.5 to 3.5 W cm⁻². This result can be ascribed to the exothermicity of the CO₂ methanation reaction, and the methanation reaction would become less favorable with the increased photothermal temperature.[12,42] Interestingly, this strategy can also work on Ni-supported CeO₂ (Ni@CeO₂) in photothermal CO₂ hydrogenation reaction (Fig. S11,12). Typically, the optimized Ni@CeO₂ catalyst achieves a high CH₄ production rate of 257.4 mmol g_{cat}⁻¹ h⁻¹ with 90.8% CH₄ selectivity under 2.5 W cm⁻² illumination (Fig. S12d). Both the CH₄ production rate and selectivity are substantially higher than that over Ni/CeO₂. We further conducted the isotope labeling experiment using ¹³CO₂ as the reactant to confirm the carbon source of the produced CH₄ over Ni@TiO₂ catalyst. As analyzed by gas chromatography–mass spectroscopy (GC–MS), the gaseous products (Fig. 3c) exhibit a discernible alteration in the mass-to-charge (*m/z*) signal of CH₄, transitioning from ¹²CH₄ to ¹³CH₄. This unequivocally validates that the source of the generated CH₄ is the photothermal CO₂ hydrogenation process.

To further illustrate the effectiveness of engineered SMSI in the process of photothermal CO₂ hydrogenation, Ni/TiO₂ was used as a reference to evaluate the photothermal CO₂ methanation performance under an irradiation intensity of 1.5 W cm⁻². As shown in Fig. 2d and S13, the CH₄ production rate (4.7 mmol g_{cat}⁻¹ h⁻¹) and CH₄ selectivity (52.3%) of Ni/TiO₂ are lower than those of the Ni@TiO₂ catalyst. These results solidly suggest that strong SMSI between Ni NPs and TiO₂ plays a fundamental role in improving both CO₂ methanation activity and selectivity. In addition, the durability of Ni@TiO₂ catalyst was then assessed through the cyclic test. We found that both the CH₄ production rate and selectivity of photothermal CO₂ methanation over Ni@TiO₂ were well maintained over the 20 successive cycles (Fig. S14 and S15).

3.3. Mechanism investigation

In order to further investigate the strong interaction between Ni NPs and TiO₂ support, Bader charge analysis was carried out to study the electron transfer between Ni and TiO₂. As shown in Fig. 4a, electrons would transfer from Ni₁₃ cluster to TiO₂ as revealed by calculated difference charge density due to the mutual interaction, and the charge transfer is determined to be 0.41 electrons through quantitative Bader analysis. To gain further insight into the role of SMSI in photothermal CO₂ hydrogenation, density functional theory (DFT) calculations were then conducted to investigate the energy change of each elementary step (Fig. 4b,c, S16, and S17). As demonstrated in Fig. 4b, the adsorbed CO₂ molecule would be first transformed into *COOH species on the catalyst surface, whose formation energy is –0.85 and 0.01 eV over the surfaces of Ni₁₃ @TiO₂ and Ni (111), respectively. Then *COOH intermediates would be further transformed into *CO species, generally thought to be the rate-determining step for CO₂ methanation reaction.[13,43] Impressively, the adsorption of *CO was found to be much stronger on the surface of Ni₁₃ @TiO₂ (–1.60 eV) compared to the Ni (111) surface (–0.98 eV). The intense adsorption of *CO species is greatly beneficial to the further hydrogenation into methane rather than for the desorption of CO molecule from the surface. In other words, the strong interaction between Ni NPs and TiO₂ in Ni@TiO₂ could substantially stabilize the *CO intermediates for deep hydrogenation of CO₂. Subsequently, the intermediates would undergo a stepwise hydrogenation pathway into CH₄ production. More importantly, these DFT calculated results can be further confirmed by CO temperature-programmed desorption (CO-TPD) tests. As shown in Fig. 4d, the CO-TPD profile for Ni@TiO₂ catalyst exhibits two predominant desorption peaks at 198 and 370 °C, which can be attributed to the physically and chemically adsorbed CO molecule, respectively. In contrast, the referenced Ni NPs shows the chemically adsorbed CO at the appreciably lower desorption peak at 315 °C. This finding also suggests that the strong interaction between Ni and TiO₂ in Ni@TiO₂ could enhance *CO adsorption for further hydrogenation.

Additionally, the adsorption behavior of CO₂ molecules was also investigated using DFT calculation. It turns out that the adsorption energy of CO₂ on Ni₁₃ @TiO₂ is –1.13 eV while the adsorption energy of CO₂ on Ni (111) is –0.11 eV (shown in Fig. 4c). These results manifest that the strong interaction between Ni NPs and TiO₂ can greatly enhance the adsorption energy of CO₂ on the surface, facilitating CO₂ adsorption for photothermal hydrogenation. Then CO₂ temperature-programmed desorption (CO₂-TPD) characterization was evaluated to experimentally observe the influence of interaction between Ni NPs and TiO₂ on CO₂ adsorption properties. The CO₂-TPD profiles (Fig. 4e) show a weak peak (197 °C) and a strong peak (379 °C) for Ni@TiO₂, indicating efficient CO₂ adsorption. Notably, the peaks for Ni NPs move toward a lower temperature (340 °C) than that of Ni@TiO₂, which indicates a stronger CO₂ adsorption and activation, consistent with the DFT calculations. Furthermore, CH₄ temperature-programmed desorption (CH₄-TPD) characterization was evaluated to experimentally observe the CH₄ adsorption properties over various catalysts. As illustrated in Fig. S18, the CH₄-TPD profile for Ni@TiO₂ catalyst exhibits a strong CH₄ desorption peak at 120, 220, and 315 °C, while Ni NPs show broad CH₄ desorption peaks at 248 and 337 °C, respectively. These observations suggest the enhanced strength of CH₄ desorption ability upon the formation of SMSI between Ni NPs and TiO₂.

To reveal the reaction pathway of CO₂ methanation over Ni@TiO₂, *in situ* diffuse reflectance infrared Fourier-transform spectroscopy (DRIFTS) was conducted to probe the intermediates of photothermal CO₂ hydrogenation. As demonstrated in Fig. 4f, the distinct peaks at 1328 and 1369 cm⁻¹ gradually strengthen in the dark, which can be assigned to the monodentate formate (m-HCOO) and bidentate formate (b-HCOO) originating from CO₂ adsorption on the surface, respectively. [44–46] Moreover, the steadily grown peaks at 1615 and 1784 cm⁻¹ can be ascribed to carbonate (CO₃²⁻) species,[45,47] indicating the efficient

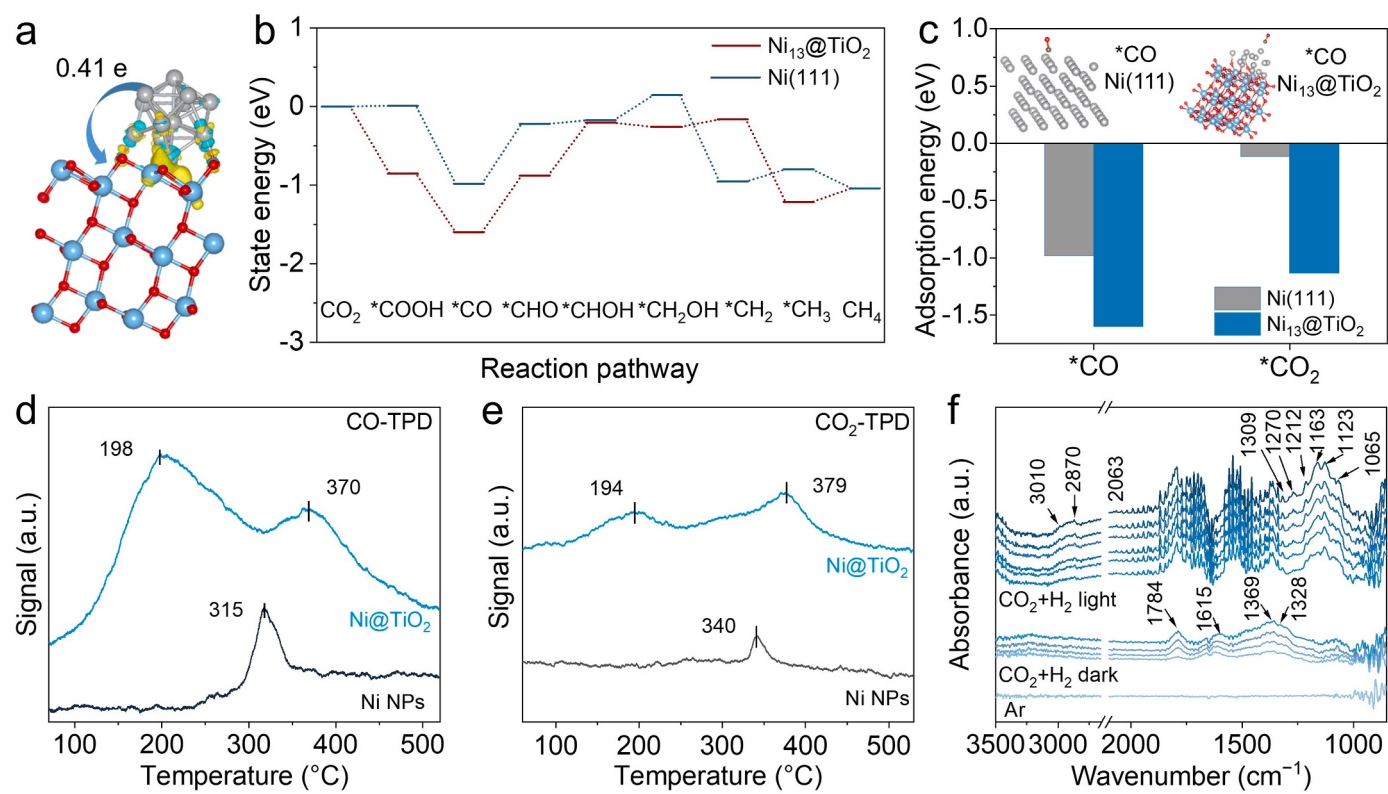


Fig. 4. (a) The calculated difference charge density for Ni₁₃@TiO₂ hybrid. (b) DFT calculated potential energy profiles for CO₂ methanation over Ni NPs and Ni₁₃@TiO₂ models. (c) The adsorption energy of CO and CO₂ molecules on Ni (111) surface and Ni₁₃@TiO₂ model. The insets are the optimized CO adsorption configuration on Ni (111) surface and Ni₁₃@TiO₂ model. (d) CO-TPD and (e) CO₂-TPD profiles of Ni@TiO₂ and Ni NPs catalysts. (f) In situ DRIFTS over Ni@TiO₂ catalyst in the dark and under full-spectrum light irradiation (2 W cm⁻²) in the atmosphere of CO₂ and H₂ (20/80 vol%) mixture with the reference in Ar atmosphere.

adsorption of CO₂ molecules on the surface of Ni@TiO₂. Upon light irradiation, the signals corresponding to adsorbed *CO ($\sim 2063\text{ cm}^{-1}$), *CHO (1065 cm^{-1}), and C-H (1123 cm^{-1}) intermediates can be obviously detected. These signals gradually grow upon illumination in the DRIFTS spectra, firmly manifesting the formation of the key intermediates in the process of photothermal CO₂ methanation.^[19,44,48] Moreover, additional peaks at 1163 and 2870 cm⁻¹ attributed to *CH₃ species appear and gradually grow, which solidly evidences the stepwise hydrogenation of the intermediates.^[49,50] More importantly, the C-H signals of CH₄ can also be appreciably observed at 1309 and 3010 cm⁻¹, and the peaks gradually strengthen with the irradiation duration.^[15,51,52] This suggests the stable production of CH₄ from photothermal CO₂ methanation over Ni@TiO₂ catalyst. Notably, additional peaks located at 1212 cm⁻¹ and broad peaks at 1640 and 1520 cm⁻¹ are attributed to the OH bending and diagnostic vibrational modes of as-formed H₂O, respectively, while the peak at 1270 cm⁻¹ can be assigned to the adsorbed H₂O on the surface,^[53–55] firmly suggesting the proceeding of Sabatier reaction. In short, the photothermal CO₂ methanation over Ni@TiO₂ is conducted via a stepwise hydrogenation pathway.

4. Conclusion

In summary, we demonstrated the strong metal-support interactions in Ni nanoparticles supported on TiO₂ (Ni@TiO₂) prepared through in situ photoreduction strategy for photothermal CO₂ hydrogenation. The interaction between Ni and TiO₂ can substantially alter the CO₂ hydrogenation pathway toward CH₄ production. Moreover, the SMSI can greatly facilitate CO₂ adsorption and CH₄ desorption on the catalyst surface. As a result, the optimized catalyst Ni@TiO₂ achieves a high CH₄ production rate of 286.5 mmol g_{cat}⁻¹ h⁻¹ with 81.8% selectivity under light illumination without additional heat source, which is much higher than that over Ni NPs (CH₄ production rate of 17.9 mmol g_{cat}⁻¹ h⁻¹ with a

10.8% selectivity). Moreover, the Ni@TiO₂ catalyst exhibits significant catalytic durability during 20 cyclic tests. Furthermore, according to the DFT, TPD and in situ DRIFTS characterizations, the adsorbed CO and *CHO species are proposed to be the essential intermediates for CO₂ methanation over Ni@TiO₂. Overall, this work provides a promising strategy to govern efficient CO₂ conversion by using renewable solar energy.

CRediT authorship contribution statement

Jun Ma: Methodology, Investigation, Data analysis, Writing – Original Draft. **Tianyang Liu:** DFT calculation. **Guangyu Chen:** Experiment, Formal analysis. **Shengkun Liu:** Data analysis. **Wanbing Gong:** Data analysis. **Yu Bai:** Experiment. **Hengjie Liu:** Experiment, Data analysis. **Yu Wang:** DFT calculation, Review & Editing. **Dong Liu:** Methodology, Writing-Review & Editing, Supervision. **Ran Long:** Methodology, Data analysis. **Yujie Xiong:** Conceptualization, Writing-Review & Editing, Supervision, Project administration, Funding acquisition.

Declaration of Competing Interest

The authors declare that they have no known competing financial interests or personal relationships that could have appeared to influence the work reported in this paper.

Data Availability

Data will be made available on request.

Acknowledgements

We acknowledge financial support from the National Key R&D Program of China (2020YFA0406103), NSFC (21725102, 22279128, 22203044, 22122506, 22075267, 21950410514, 51902311), Strategic Priority Research Program of the CAS (XDPB14), Anhui Provincial Natural Science Foundation (2008085J05), Youth Innovation Promotion Association of CAS (2019444), China Postdoctoral Science Foundation (2021M703122), Jiangsu Funding Program for Excellent Postdoctoral Talent, Jiangsu Specially Appointed Professor Plan, Gusu Innovation and Entrepreneurship Leading Talents Program (ZXL2022386), Science and Technology Program of Suzhou (SWY2022003) and Fundamental Research Funds for the Central Universities (WK2060000039, 20720220007). In situ DRIFTS measurements were performed at the Infrared Spectroscopy and Microspectroscopy Endstation (BL01B) of NSRL. We thank the support from USTC Center for Micro-and Nanoscale Research and Fabrication.

Appendix A. Supplementary data

Supplementary data associated with this article can be found in the online version.

Appendix A. Supporting information

Supplementary data associated with this article can be found in the online version at [doi:10.1016/j.apcatb.2023.123600](https://doi.org/10.1016/j.apcatb.2023.123600).

References

- [1] E. Gong, S. Ali, C.B. Hiragond, H.S. Kim, N.S. Powar, D. Kim, H. Kim, S.-I. In, Solar fuels: research and development strategies to accelerate photocatalytic CO₂ conversion into hydrocarbon fuels, *Energy Environ. Sci.* 15 (2022) 880–937, <https://doi.org/10.1039/D1EE02714J>.
- [2] M.A.A. Aziz, A.A. Jalil, S. Triwahyono, A. Ahmad, CO₂ methanation over heterogeneous catalysts: recent progress and future prospects, *Green. Chem.* 17 (2015) 2647–2663, <https://doi.org/10.1039/C5GC00119F>.
- [3] J. Arzt, T.E. Müller, K. Thenert, J. Kleinekorte, R. Meyn, A. Sternberg, A. Bardow, W. Leitner, Sustainable conversion of carbon dioxide: an integrated review of catalysis and life cycle assessment, *Chem. Rev.* 118 (2018) 434–504, <https://doi.org/10.1021/acs.chemrev.7b00435>.
- [4] J. Low, J. Ma, J. Wan, W. Jiang, Y. Xiong, Identification and design of active sites on photocatalysts for the direct artificial carbon cycle, *Acc. Mater. Res.* 3 (2022) 331–342, <https://doi.org/10.1021/accountsmr.1c00222>.
- [5] C. Gao, J. Low, R. Long, T. Kong, J. Zhu, Y. Xiong, Heterogeneous single-atom photocatalysts: fundamentals and applications, *Chem. Rev.* 120 (2020) 12175–12216, <https://doi.org/10.1021/acs.chemrev.9b00840>.
- [6] J.L. White, M.F. Baruch, J.E. Pander, III, Y. Hu, I.C. Fortmeyer, J.E. Park, T. Zhang, K. Liao, J. Gu, Y. Yan, T.W. Shaw, E. Abelev, A.B. Bocarsly, Light-driven heterogeneous reduction of carbon dioxide: photocatalysts and photoelectrodes, *Chem. Rev.* 115 (2015) 12888–12935, <https://doi.org/10.1021/acs.chemrev.5b00370>.
- [7] Y. Dong, P. Duchesne, A. Mohan, K.K. Ghuman, P. Kant, L. Hurtado, U. Ulmer, J.Y. Y. Loh, A.A. Tountas, L. Wang, A. Jelle, M. Xia, R. Dittmeyer, G.A. Ozin, Shining light on CO₂: from materials discovery to photocatalyst, photoreactor and process engineering, *Chem. Soc. Rev.* 49 (2020) 5648–5663, <https://doi.org/10.1039/DOCS00597E>.
- [8] M. Cai, Z. Wu, Z. Li, L. Wang, W. Sun, A.A. Tountas, C. Li, S. Wang, K. Feng, A.-B. Xu, S. Tang, A. Tavasoli, M. Peng, W. Liu, A.S. Helmy, L. He, G.A. Ozin, X. Zhang, Greenhouse-inspired supra-photothermal CO₂ catalysis, *Nat. Energy* 6 (2021) 807–814, <https://doi.org/10.1038/s41560-021-00867-w>.
- [9] G. Chen, R. Gao, Y. Zhao, Z. Li, G.I.N. Waterhouse, R. Shi, J. Zhao, M. Zhang, L. Shang, G. Sheng, X. Zhang, X. Wen, L.-Z. Wu, C.-H. Tung, T. Zhang, Alumina-supported CoFe alloy catalysts derived from layered-double-hydroxide nanosheets for efficient photothermal CO₂ hydrogenation to hydrocarbons, *Adv. Mater.* 30 (2018), 1704663. (<https://onlinelibrary.wiley.com/doi/abs/10.1002/adma.201704663>).
- [10] J. Ma, J. Yu, G. Chen, Y. Bai, S. Liu, Y. Hu, M. Al-Mamun, Y. Wang, W. Gong, D. Liu, Y. Li, R. Long, H. Zhao, Y. Xiong, Rational design of N-doped carbon coated cobalt nanoparticles for highly efficient and durable photothermal CO₂ conversion, *Adv. Mater.* (2023), 2302537, <https://doi.org/10.1002/adma.202302537>.
- [11] X. Meng, T. Wang, L. Liu, S. Ouyang, P. Li, H. Hu, T. Kako, H. Iwai, A. Tanaka, J. Ye, Photothermal conversion of CO₂ into CH₄ with H₂ over GroupVIII nanocatalysts: an alternative approach for solar fuel production, *Angew. Chem. Int. Ed.* 53 (2014) 11478–11482. (<https://onlinelibrary.wiley.com/doi/abs/10.1002/anie.201404953>).
- [12] G. Fu, M. Jiang, J. Liu, K. Zhang, Y. Hu, Y. Xiong, A. Tao, Z. Tie, Z. Jin, Rh/Al nanoantenna photothermal catalyst for wide-spectrum solar-driven CO₂ methanation with nearly 100% selectivity, *Nano Lett.* 21 (2021) 8824–8830, <https://doi.org/10.1021/acs.nanolett.1c03215>.
- [13] Y. Guo, S. Mei, K. Yuan, D.-J. Wang, H.-C. Liu, C.-H. Yan, Y.-W. Zhang, Low-temperature CO₂ methanation over CeO₂-supported Ru single atoms, nanoclusters, and nanoparticles competitively tuned by strong metal-support interactions and H-spillover effect, *ACS Catal.* 8 (2018) 6203–6215, <https://doi.org/10.1021/acscatal.7b04469>.
- [14] X. Wang, H. Shi, J. Szanyi, Controlling selectivities in CO₂ reduction through mechanistic understanding, *Nat. Commun.* 8 (2017), 513, <https://doi.org/10.1038/s41467-017-00558-9>.
- [15] Y. Chen, Y. Zhang, G. Fan, L. Song, G. Jia, H. Huang, S. Ouyang, J. Ye, Z. Li, Z. Zou, Cooperative catalysis coupling photo-/photothermal effect to drive Sabatier reaction with unprecedented conversion and selectivity, *Joule* 5 (2021) 3235–3251. (<https://www.sciencedirect.com/science/article/pii/S254243512005353>).
- [16] J. Ren, S. Ouyang, H. Xu, X. Meng, T. Wang, D. Wang, J. Ye, Targeting activation of CO₂ and H₂ over Ru-loaded ultrathin layered double hydroxides to achieve efficient photothermal CO₂ methanation in flow-type system, *Adv. Energy Mater.* 7 (2017), 1601657, <https://doi.org/10.1002/aenm.201601657>.
- [17] Z. Wu, J. Shen, C. Li, C. Zhang, K. Feng, Z. Wang, X. Wang, D.M. Meira, M. Cai, D. Zhang, S. Wang, M. Chu, J. Chen, Y. Xi, L. Zhang, T.-K. Sham, A. Genest, G. Rupprecht, X. Zhang, L. He, Mo₂TiC₂ MXene-supported Ru clusters for efficient photothermal reverse water-gas shift, *ACS Nano* 17 (2023) 1550–1559, <https://doi.org/10.1021/acsnano.2c10707>.
- [18] H. Jiang, L. Wang, H. Kaneko, R. Gu, G. Su, L. Li, J. Zhang, H. Song, F. Zhu, A. Yamaguchi, J. Xu, F. Liu, M. Miyachi, W. Ding, M. Zhong, Light-driven CO₂ methanation over Au-grafted Ce0.95Ru0.05O₂ solid-solution catalysts with activities approaching the thermodynamic limit, *Nat. Catal.* 6 (2023) 519–530, <https://doi.org/10.1038/s41929-023-00970-z>.
- [19] S. Kattel, W. Yu, X. Yang, B. Yan, Y. Huang, W. Wan, P. Liu, J.G. Chen, CO₂ hydrogenation over oxide-supported PtCo catalysts: the role of the oxide support in determining the product selectivity, *Angew. Chem. Int. Ed.* 55 (2016) 7968–7973. (<https://onlinelibrary.wiley.com/doi/abs/10.1002/anie.201601661>).
- [20] Z. Jia, S. Ning, Y. Tong, X. Chen, H. Hu, L. Liu, J. Ye, D. Wang, Selective photothermal reduction of CO₂ to CO over Ni-nanoparticle/N-doped CeO₂ nanocomposite catalysts, *ACS Appl. Nano Mater.* 4 (2021) 10485–10494, <https://doi.org/10.1021/acsanm.1c01991>.
- [21] J. Gong, M. Chu, W. Guan, Y. Liu, Q. Zhong, M. Cao, Y. Xu, Regulating the interfacial synergy of Ni/Ga₂O₃ for CO₂ hydrogenation toward the reverse water-gas shift reaction, *Ind. Eng. Chem. Res.* 60 (2021) 9448–9455, <https://doi.org/10.1021/acs.iecr.0c05495>.
- [22] Y.-F. Xu, P.N. Duchesne, L. Wang, A. Tavasoli, A.A. Jelle, M. Xia, J.-F. Liao, D.-B. Kuang, G.A. Ozin, High-performance light-driven heterogeneous CO₂ catalysis with near-unity selectivity on metal phosphides, *Nat. Commun.* 11 (2020), 5149, <https://doi.org/10.1038/s41467-020-18943-2>.
- [23] K. Feng, S. Wang, D. Zhang, L. Wang, Y. Yu, K. Feng, Z. Li, Z. Zhu, C. Li, M. Cai, Z. Wu, N. Kong, B. Yan, J. Zhong, X. Zhang, G.A. Ozin, L. He, Cobalt plasmonic superstructures enable almost 100% broadband photon efficient CO₂ photocatalysis, *Adv. Mater.* 32 (2020), 2000014, <https://doi.org/10.1002/adma.202000014>.
- [24] X. Li, J. Lin, L. Li, Y. Huang, X. Pan, S.E. Collins, Y. Ren, Y. Su, L. Kang, X. Liu, Y. Zhou, H. Wang, A. Wang, B. Qiao, X. Wang, T. Zhang, Controlling CO₂ hydrogenation selectivity by metal-supported electron transfer, *Angew. Chem. Int. Ed.* 59 (2020) 19983–19989. (<https://onlinelibrary.wiley.com/doi/abs/10.1002/anie.202003847>).
- [25] M.D. Porosoff, B. Yan, J.G. Chen, Catalytic reduction of CO₂ by H₂ for synthesis of CO, methanol and hydrocarbons: challenges and opportunities, *Energy Environ. Sci.* 9 (2016) 62–73, <https://doi.org/10.1039/C5EE02657A>.
- [26] C. Wang, E. Guan, L. Wang, X. Chu, Z. Wu, J. Zhang, Z. Yang, Y. Jiang, L. Zhang, X. Meng, B.C. Gates, F.-S. Xiao, Product selectivity controlled by nanoporous environments in zeolite crystals enveloping rhodium nanoparticle catalysts for CO₂ hydrogenation, *J. Am. Chem. Soc.* 141 (2019) 8482–8488, <https://doi.org/10.1021/jacs.9b01555>.
- [27] J. Ma, C. Zhu, K. Mao, W. Jiang, J. Low, D. Duan, H. Ju, D. Liu, K. Wang, Y. Zang, S. Chen, H. Zhang, Z. Qi, R. Long, Z. Liu, L. Song, Y. Xiong, Sustainable methane utilization technology via photocatalytic halogenation with alkali halides, *Nat. Commun.* 14 (2023), 1410, <https://doi.org/10.1038/s41467-023-36977-0>.
- [28] X. Wang, H. Shi, J.H. Kwak, J. Szanyi, Mechanism of CO₂ hydrogenation on Pd/Al₂O₃ catalysts: kinetics and transient DRIFTS-MS studies, *ACS Catal.* 5 (2015) 6337–6349, <https://doi.org/10.1021/acscatal.5b01464>.
- [29] A. Beck, X. Huang, L. Artiglia, M. Zabilskiy, X. Wang, P. Rzepka, D. Palagin, M.-G. Willinger, J.A. van Bokhoven, The dynamics of overlayer formation on catalyst nanoparticles and strong metal-support interaction, *Nat. Commun.* 11 (2020), 3220, <https://doi.org/10.1038/s41467-020-17070-2>.
- [30] X. Liu, M.-H. Liu, Y.-C. Luo, C.-Y. Mou, S.D. Lin, H. Cheng, J.-M. Chen, J.-F. Lee, T.-S. Lin, Strong metal-support interactions between gold nanoparticles and ZnO nanorods in CO oxidation, *J. Am. Chem. Soc.* 134 (2012) 10251–10258, <https://doi.org/10.1021/ja3033235>.
- [31] T. Lunkenbein, J. Schumann, M. Behrens, R. Schlögl, M.G. Willinger, Formation of a ZnO overlayer in industrial Cu/ZnO/Al₂O₃ catalysts induced by strong metal-support interactions, *Angew. Chem. Int. Ed.* 54 (2015) 4544–4548, <https://doi.org/10.1002/anie.201411581>.
- [32] H. Xin, L. Lin, R. Li, D. Li, T. Song, R. Mu, Q. Fu, X. Bao, Overturning CO₂ hydrogenation selectivity with high activity via reaction-induced strong

- metal-support interactions, *J. Am. Chem. Soc.* 144 (2022) 4874–4882, <https://doi.org/10.1021/jacs.1c12603>.
- [33] J. Dong, Q. Fu, H. Li, J. Xiao, B. Yang, B. Zhang, Y. Bai, T. Song, R. Zhang, L. Gao, J. Cai, H. Zhang, Z. Liu, X. Bao, Reaction-induced strong metal-support interactions between metals and inert boron nitride nanosheets, *J. Am. Chem. Soc.* 142 (2020) 17167–17174, <https://doi.org/10.1021/jacs.0c08139>.
- [34] J.C. Matsubu, S. Zhang, L. DeRita, N.S. Marinkovic, J.G. Chen, G.W. Graham, X. Pan, P. Christopher, Adsorbate-mediated strong metal-support interactions in oxide-supported Rh catalysts, *Nat. Chem.* 9 (2017) 120–127, <https://doi.org/10.1038/nchem.2607>.
- [35] S.-W. Ho, C.-Y. Chu, S.-G. Chen, Effect of thermal treatment on the nickel state and CO hydrogenation activity of titania-supported nickel catalysts, *J. Catal.* 178 (1998) 34–48. (<https://www.sciencedirect.com/science/article/pii/S0021951798921029>).
- [36] S. Yao, X. Wang, Y. Jiang, F. Wu, X. Chen, X. Mu, One-step conversion of biomass-derived 5-hydroxymethylfurfural to 1,2,6-hexanetriol over Ni–Co–Al mixed oxide catalysts under mild conditions, *ACS Sustain. Chem. Eng.* 2 (2014) 173–180, <https://doi.org/10.1021/sc4003714>.
- [37] H. Chen, Z. Yang, X. Wang, F. Polo-Garzon, P.W. Halstenberg, T. Wang, X. Suo, S.-Z. Yang, H.M. Meyer, III, Z. Wu, S. Dai, Photoinduced strong metal-support interaction for enhanced catalysis, *J. Am. Chem. Soc.* 143 (2021) 8521–8526, <https://doi.org/10.1021/jacs.0c12817>.
- [38] T.W. van Deelen, C. Hernández Mejía, K.P. de Jong, Control of metal-support interactions in heterogeneous catalysts to enhance activity and selectivity, *Nat. Catal.* 2 (2019) 955–970, <https://doi.org/10.1038/s41929-019-0364-x>.
- [39] W. Lin, H. Cheng, L. He, Y. Yu, F. Zhao, High performance of Ir-promoted Ni/TiO₂ catalyst toward the selective hydrogenation of cinnamaldehyde, *J. Catal.* 303 (2013) 110–116. (<https://www.sciencedirect.com/science/article/pii/S0021951713000870>).
- [40] H. Zhang, T. Wang, J. Wang, H. Liu, T.D. Dao, M. Li, G. Liu, X. Meng, K. Chang, L. Shi, T. Nagao, J. Ye, Surface-plasmon-enhanced photodriven CO₂ reduction catalyzed by metal–organic-framework-derived iron nanoparticles encapsulated by ultrathin carbon layers, *Adv. Mater.* 28 (2016) 3703–3710. (<https://onlinelibrary.wiley.com/doi/abs/10.1002/adma.201505187>).
- [41] D. Liu, C. Xue, Plasmonic coupling architectures for enhanced photocatalysis, *Adv. Mater.* 33 (2021), 2005738, <https://doi.org/10.1002/adma.202005738>.
- [42] C. Song, X. Liu, M. Xu, D. Masi, Y. Wang, Y. Deng, M. Zhang, X. Qin, K. Feng, J. Yan, J. Leng, Z. Wang, Y. Xu, B. Yan, S. Jin, D. Xu, Z. Yin, D. Xiao, D. Ma, Photothermal conversion of CO₂ with tunable selectivity using Fe-based catalysts: from oxide to carbide, *ACS Catal.* 10 (2020) 10364–10374, <https://doi.org/10.1021/acscatal.0c02244>.
- [43] B. Miao, S.S.K. Ma, X. Wang, H. Su, S.H. Chan, Catalysis mechanisms of CO₂ and CO methanation, *Catal. Sci. Techn.* 6 (2016) 4048–4058, <https://doi.org/10.1039/C6CY00478D>.
- [44] Q. Li, Y. Gao, M. Zhang, H. Gao, J. Chen, H. Jia, Efficient infrared-light-driven photothermal CO₂ reduction over MOF-derived defective Ni/TiO₂, *Appl. Catal. B* 303 (2022), 120905. (<https://www.sciencedirect.com/science/article/pii/S09237321010304>).
- [45] Y.F. Li, N. Soheilnia, M. Greiner, U. Ulmer, T. Wood, F.M. Ali, Y. Dong, A.P. Yin Wong, J. Jia, G.A. Ozin, Pd@HyWO₃-x nanowires efficiently catalyze the CO₂ heterogeneous reduction reaction with a pronounced light effect, *ACS Appl. Mater. Interfaces* 11 (2019) 5610–5615, <https://doi.org/10.1021/acsami.8b04982>.
- [46] R.-P. Ye, Q. Li, W. Gong, T. Wang, J.J. Razink, L. Lin, Y.-Y. Qin, Z. Zhou, H. Adidharma, J. Tang, A.G. Russell, M. Fan, Y.-G. Yao, High-performance of nanostructured Ni/CeO₂ catalyst on CO₂ methanation, *Appl. Catal. B* 268 (2020), 118474. (<https://www.sciencedirect.com/science/article/pii/S0926337319312202>).
- [47] L. Liu, Y. Jiang, H. Zhao, J. Chen, J. Cheng, K. Yang, Y. Li, Engineering coexposed {001} and {101} facets in oxygen-deficient TiO₂ nanocrystals for enhanced CO₂ photoreduction under visible light, *ACS Catal.* 6 (2016) 1097–1108, <https://doi.org/10.1021/acscatal.5b02098>.
- [48] X. Li, Y. Sun, J. Xu, Y. Shao, J. Wu, X. Xu, Y. Pan, H. Ju, J. Zhu, Y. Xie, Selective visible-light-driven photocatalytic CO₂ reduction to CH₄ mediated by atomically thin CuInS₂ layers, *Nat. Energy* 4 (2019) 690–699, <https://doi.org/10.1038/s41560-019-0431-1>.
- [49] J. Ma, K. Mao, J. Low, Z. Wang, D. Xi, W. Zhang, H. Ju, Z. Qi, R. Long, X. Wu, L. Song, Y. Xiong, Efficient photoelectrochemical conversion of methane into ethylene glycol by WO₃ nanobar arrays, *Angew. Chem. Int. Ed.* 60 (2021) 9357–9361, <https://doi.org/10.1002/anie.202101701>.
- [50] J. Kim, A. Dutta, B. Memarzadeh, A.V. Kildishev, H. Mosallaei, A. Boltasseva, Zinc oxide based plasmonic multilayer resonator: localized and gap surface plasmon in the infrared, *ACS Photonics* 2 (2015) 1224–1230, <https://doi.org/10.1021/acspophotonics.5b00318>.
- [51] J. Ma, J. Low, D. Wu, W. Gong, H. Liu, D. Liu, R. Long, Y. Xiong, Cu and Si co-doping on TiO₂ nanosheets to modulate reactive oxygen species for efficient photocatalytic methane conversion, *Nanoscale Horiz.* 8 (2023) 63–68, <https://doi.org/10.1039/D2NH00457G>.
- [52] X. Yan, W. Sun, L. Fan, P.N. Duchesne, W. Wang, C. Kübel, D. Wang, S.G.H. Kumar, Y.F. Li, A. Tavasoli, T.E. Wood, D.L.H. Hung, L. Wan, L. Wang, R. Song, J. Guo, I. Gourevich, F.M. Ali, J. Lu, R. Li, B.D. Hatton, G.A. Ozin, Nickel@Siloxene catalytic nanosheets for high-performance CO₂ methanation, *Nat. Commun.* 10 (2019), 2608, <https://doi.org/10.1038/s41467-019-10464-x>.
- [53] J.C. Lavalle, M. Bensitel, J.P. Gallas, J. Lamotte, G. Busca, V. Lorenzelli, FT-IR study of the δ(OH) mode of surface hydroxy groups on metal oxides, *J. Mol. Struct.* 175 (1988) 453–458. (<https://www.sciencedirect.com/science/article/pii/S0022286098801191>).
- [54] W. Jiang, J. Low, K. Mao, D. Duan, S. Chen, W. Liu, C.-W. Pao, J. Ma, S. Sang, C. Shu, X. Zhan, Z. Qi, H. Zhang, Z. Liu, X. Wu, R. Long, L. Song, Y. Xiong, Pd-modified ZnO–Au enabling alkoxy intermediates formation and dehydrogenation for photocatalytic conversion of methane to ethylene, *J. Am. Chem. Soc.* 143 (2021) 269–278, <https://doi.org/10.1021/jacs.0c10369>.
- [55] C. Vogt, M. Monai, E.B. Sterk, J. Palle, A.E.M. Melcherts, B. Zijlstra, E. Groeneveld, P.H. Berben, J.M. Boereboom, E.J.M. Hensen, F. Meirer, I.A.W. Filot, B. M. Weckhuysen, Understanding carbon dioxide activation and carbon–carbon coupling over nickel, *Nat. Commun.* 10 (2019), 5330, <https://doi.org/10.1038/s41467-019-12858-3>.